

***Retracted:* BAYESIAN LINEARIZED INVERSION FOR PETROPHYSICAL AND PORE-CONNECTIVITY PARAMETERS WITH SEISMIC ELASTIC DATA OF CARBONATE RESERVOIRS**

JING BA¹, JIAWEI CHEN¹, QIANG GUO^{2,1*}, XIAO CHEN³, XINFEI YAN⁴, ZHIJIAN FANG¹

¹*School of Earth Sciences and Engineering, Hohai University, Nanjing 211100, China*

²*School of Resources and Geosciences, China University of Mining and Technology, Xuzhou 221116, China*

³*Research Institute of Petroleum Exploration and Development, PetroChina Southwest Oil & Gasfield Company, Chengdu 610212, China*

⁴*Research Institute of Petroleum Exploration and Development, PetroChina, Beijing 100083, China*

(Received February 8, 2022; revised version accepted December 20, 2022)

ABSTRACT

Carbonate reservoirs are important targets for promoting the oil and gas reserve exploration and production in China. However, such reservoirs usually contain the developed complex pore structures, which heavily affect the precision in seismic prediction of petrophysical parameters. As one of the most important parameters to characterize reservoir rock, pore parameters can not only describe the pore structure, but also be used to evaluate the oil/gas bearing capabilities of potential reservoirs. The conventional rock-physics models (such as the Gassmann model) are established under the assumption of fully-connected pores, which cannot reasonably describe the geometrical complexity of real rocks. To characterize the effects of different pore types on the elastic moduli, this work proposes a rock-physics modeling method for carbonates, where the volume content of connected pores (defined as the pore-connectivity parameter) is quantified. The proposed method treats the pore-connectivity parameter as an objective parameter to characterize the spatial variations of pore structure. Specifically, the method combines the differential equivalent medium theory and the Gassmann model, and derives a linearized forward operator to quantitatively relate porosity, fluid saturation, and pore-connectivity parameter to the seismic elastic parameters. Based on the Bayesian linear inverse theory, the simultaneous inversion for petrophysical and pore-connectivity parameters are achieved. To characterize the statistical variations within the lithofacies, the Gaussian mixture model is introduced to describe the prior distribution of the objective parameters. The analytical expression for the posterior distribution of the objective parameters is obtained with the linearized forward operator. Numerical tests indicate that the accuracy of predicted elastic parameters by the proposed method is improved compared with the conventional Xu-White model and the varying pore aspect ratio method. The application to the field data validates the effectiveness of the method, wherein the porosity and fluid saturation results help indicating the spatial distribution of potential reservoirs.

KEY WORDS: carbonate reservoirs; DEM model; Gassmann model; the Xu-White model; Bayesian linear inversion; Gaussian mixture model

INTRODUCTION

As most of the clastic oil and gas fields have faced the middle and late production stages, the exploration and development of carbonate reservoirs are gaining increasing attentions (Cao *et al.* 2018). However, due to the sedimentation, diagenesis, and tectonic factors in the formation process, carbonates usually exhibit strong heterogeneity with non-uniform mineral distribution and internal properties, which may lead to the complex pore structures/types (Xu and Payne 2009; Gharechelou *et al.* 2015). The pore complexity in carbonate reservoirs poses significant challenges for seismic/elastic predictions with conventional rock-physics modeling/inversion methods (Falahat and Farrokhnia 2020; Zhang *et al.* 2022). The pore structure/type (e.g., connectivity, geometry, etc.) has been demonstrated to be the significant factors that influence the elastic properties of carbonates (Assefa *et al.* 2003; Mirkamali *et al.* 2020; Garia *et al.* 2021). Therefore, to provide a more accurate description of the potential reservoirs, it is essential to consider the impacts of different pore types in modeling approaches.

To describe the compositions and structures of real rocks, the rock-physics model establishes theoretical frameworks for quantifying the internal correlations between elastic and reservoir-property parameters of rocks, which provides a fundamental basis for probing into the seismic petrophysical forward modeling and inversion (Keys and Xu 2002; Mavko *et al.* 2013; Ba *et al.* 2017). The rock can be assumed as a complex porous multiphase medium consisting of minerals, pore spaces, and fluid within these pores. Therefore, reservoir rocks can be simplified as equivalent mediums to investigate the elastic or petrophysical characteristics based on the mathematical and physical principles. For the estimation of the equivalent elastic moduli of solid rocks, various well-established rock-physics models have been developed, for example, the Voigt-Reuss-Hill average (Hill 1952), the Kuster-Toksöz model for the sparsely distributed inclusions (Kuster and Toksöz 1974), the self-consistent model (Berryman 1980), and the differential equivalent medium (DEM) model (Cleary *et al.* 1980; Norris 1985; Zimmerman 1985). In consideration of the impact of pore fluid, Gassmann (1951) proposed the equations of elastic moduli of saturated porous rocks and formulated the Gassmann equations, which have been extensively applied for predicting the elastic properties of fluid-saturated rocks. In particular, the rock-physics modeling approach proposed by Xu and White (1995) integrated the differential equivalent medium model, Kuster-Toksöz model, and Gassmann equation to characterize the sands and mudstones. Notably, the Xu-White model introduced a simplified classification of pores into sand-related hard pores and clay-related soft pores. As an extension to the Xu-White model, Xu and Payne (2009) proposed to classify the carbonate pores as moldic, interparticle, and microcrack porosities, which addresses the multiple pore types in rock-physics modeling.

Seismic petrophysical inversion method plays a crucial role in the prediction of oil/gas reservoirs by inferring subsurface reservoir properties with recorded seismic data. Typically, the inversion requires the established petrophysical forward model, and incorporates the prior constraint information, based on which optimization algorithm is employed to achieve the estimation of model parameters. Due to the influence of model error and noise, the inversion solution is non-unique. Therefore, it is essential to express the inversion result in terms of probability distribution with quantified uncertainty for the model parameters. The Bayesian approach, which is widely used in handling geophysical inversion problems, effectively incorporates prior information into the solution and facilitates the evaluation of the result uncertainties (Gunning and Glinsky 2007; Chen *et al.* 2017; Pan *et al.* 2019; Fjeldstad and Omre 2020; Qin *et al.* 2021; Ji and Zong 2023). According to the inversion algorithm, the Bayesian approach can be categorized into the deterministic inversion and the stochastic inversion. The former usually assumes that the model parameters follow a Gaussian distribution with a linear forward operator. Based on this assumption, it is possible to derive an analytical expression for the solution of the inversion problem (i.e., the posterior expectation and covariance) (Grana *et al.* 2017; Luo *et al.* 2023). The primary objective of stochastic inversion is to address highly nonlinear inversion problems that lack any analytical expression of the solution. In the case of high nonlinearity, the solution can be obtained by inferring the likelihood function through stochastic sampling or global optimization algorithms (Yin *et al.* 2014; Azevedo *et al.* 2017). Particularly the nonlinear petrophysical forward model can also be locally linearized by using the Taylor series expansion so as to obtain the analytical representation for the Bayesian inversion (Grana 2016). Grana *et al.* (2017) proposed a Bayesian linear inversion method based on the Gaussian mixture model. This approach introduces a recursive exact formula to approximate the posterior distribution of the inversion problem, taking into account the variations in statistical distributions of model parameters with different lithofacies. In summary, deterministic inversion method provides efficient and stabilized solutions to the inversion problem. However, stochastic inversion method can handle nonlinear problem but it involves iterative sampling or optimization that often requires extensive forward computations and suffers from drawbacks such as low computational efficiency and unstable inversion results.

For seismic petrophysical inversion applications, porosity, fluid saturation, and mineral content are commonly considered as the objective variables to be estimated. Compared with the conventional sandstone reservoirs, carbonates exhibit complex pore structures, which are characterized by the coexisting of two or more distinct pore types (Weger *et al.* 2009; Bemmer *et al.* 2019). Therefore, it becomes particularly crucial to employ multiple variables for effectively characterizing these complex pore types. For instance, the pore geometry can be incorporated as an intermediate variable to assist the inversion of petrophysical parameters by Guo *et al.* (2022), which effectively characterizes the spatial

variation of pore structure in carbonate reservoirs. In addition to pore geometry, the pore connectivity affects elastic or oil/gas-bearing properties in carbonates. Ishola *et al.* (2022) demonstrated the prominent effect of pore connectivity on permeability and hydraulic bending of highly heterogeneous porous medias such as carbonate rocks with a stochastic 3D pore scale simulation method. In particular, rock permeability is proven to be largely influenced by pore geometry or structure, which leads to connected and isolated pores in carbonates (Zhang *et al.* 2022; Dias *et al.* 2023). On the other hand, rock elastic properties of pore-filling fluid with connected pores is different from those regarding isolated pores in rock-physics modeling (Carcione *et al.* 2011; Panizza and Ravazzoli 2019; Wang *et al.* 2020), e.g., the Gassmann and DEM models basically assume fully-connected and isolated pores, respectively. Therefore, for carbonate rock-physics modeling and inversion, the consideration of different pore structures and the associated connectivity is critical for improving the accuracy of reservoir prediction and characterization.

To address the aforementioned issues, we propose a rock-physics modeling and Bayesian seismic petrophysical inversion method for carbonate reservoirs. The method takes into account the combined influence of isolated and connected pores, which quantifies the percentage of connected pores as the pore connectivity parameter. By utilizing the decoupled DEM model and the Gassmann equation, the seismic rock-physics forward operator is derived to link petrophysical parameters (porosity and water saturation) and pore parameter (pore connectivity parameter) to elastic parameters (P- and S-wave velocities and density). The Gaussian mixture model is employed to characterize the prior probability distribution of the objective variables, including petrophysical and pore parameters, to capture the statistical differences among lithofacies. We derive the linearized forward operator with the Taylor expansion and obtain the analytical expression of the posterior probability distribution for the objective variables with the Bayesian linear inversion method. The proposed linearized inversion method has the advantage of computational efficiency. Particularly, the pore connectivity parameter is adopted as one of the objective variables, which assists with the characterization of pore structures and the improvement of rock-physics modeling accuracy.

METHODOLOGY AND THEORY

Rock Physics Modeling

According to the matrix-skeleton-fluid rock-physics modeling method, the modeling process of carbonate reservoirs primarily involve calculating the elastic moduli of rock matrix/pore fluid, rock skeleton, and fluid-saturated rock. The equivalent elastic moduli of rock matrix can be determined with the Voigt-

Reuss-Hill (VRH) average.

The bulk modulus K_d and shear modulus μ_d of rock skeleton can be determined with the utilization of the decoupled differential equivalent medium (DEM) model according to Keys and Xu (2002),

$$K_d = K_m (1 - \phi)^{P(\alpha)}, \quad (1)$$

$$\mu_d = \mu_m (1 - \phi)^{Q(\alpha)}, \quad (2)$$

where K_m and μ_m are the bulk and shear moduli of rock matrix, respectively, ϕ is the porosity, and P and Q are the polarization factors related to the pore aspect ratio α (Berryman 1980).

By assuming that pore fluid is the brine and hydrocarbon mixture, the fluid bulk modulus (K_f) is computed with the Wood model (Mavko *et al.* 2009),

$$K_f = \left(\frac{S_w}{K_w} + \frac{1 - S_w}{K_h} \right)^{-1}, \quad (3)$$

where S_w is water saturation, and K_w and K_h are the bulk moduli of brine and hydrocarbon, respectively. The bulk modulus K_s and shear modulus μ_s of fluid-saturated rock can be obtained by the Gassmann equation,

$$K_s = K_d + \left(1 - \frac{K_d}{K_m} \right)^2 \left(\frac{\phi}{K_f} + \frac{1 - \phi}{K_m} - \frac{K_d}{K_m^2} \right)^{-1} \quad (4)$$

$$\mu_s = \mu_d. \quad (5)$$

To consider the complex pore structures in carbonates and improve modeling accuracy, we divide the pore spaces into two parts, i.e., connected and isolated pores, based on which the percentage content of connected pores is defined (referred as the pore-connectivity parameter β). The total porosity ϕ_t is thereby partitioned into connected-pore porosity ϕ_{con} and isolated-pore porosity ϕ_{dis} , which satisfy $\phi_{con} = \beta \cdot \phi_t$ and $\phi_{dis} = (1 - \beta) \cdot \phi_t$. In practice, the elastic moduli of saturated rocks with the two types of pores are computed separately. It is considered that the connected pores represent pore spaces that are connected with each other, while the isolated pores represent sealed and isolated pores; the fluid mixture movement mainly occurs between the connected pores.

The moduli of saturated rock with connected pores are estimated by using the Gassmann equation, which follows the conventional Xu-White model,

$$K_{con} = K_{dry} + \frac{\left(1 - \frac{K_{dry}}{K_m} \right)^2}{\frac{\phi_{con}}{K_{fl}} + \frac{1 - \phi_{con}}{K_m} - \frac{K_{dry}}{K_m^2}}, \quad (6)$$

$$\mu_{\text{con}} = \mu_{\text{dry}}, \quad (7)$$

where K_{con} and μ_{con} represent the bulk and shear moduli of fluid-saturated rock with connected pores, respectively, and ϕ_{con} represents the connected-pore porosity.

Since the Gassmann model is based on the fully-connected pore assumption, we estimate the saturated rock moduli with isolated pores by the decoupled DEM model (Keys and Xu 2002),

$$K_{\text{dis}} = K_{\text{m}} (1 - \phi_{\text{dis}})^P, \quad (8)$$

$$\mu_{\text{dis}} = \mu_{\text{m}} (1 - \phi_{\text{dis}})^Q, \quad (9)$$

where K_{dis} and μ_{dis} represent the bulk and shear moduli of saturated rock with isolated pores, respectively, and ϕ_{dis} represents the isolated pore porosity. The modeling process with equations (6)-(7) and (8)-(9) are referred as the connected- and isolated-pore models, respectively.

Then, we employ the VRH average to estimate the overall elastic properties jointly affected by the connected and isolated pores, in which the two types of pores are weighted by the pore-connectivity parameter in the estimation,

$$K_{\text{cmb}} = \frac{[\beta K_{\text{con}} + (1 - \beta) K_{\text{dis}}] + \left[\frac{1}{\beta / K_{\text{con}} + (1 - \beta) / K_{\text{dis}}} \right]}{2}, \quad (10)$$

$$\mu_{\text{cmb}} = \frac{[\beta \mu_{\text{con}} + (1 - \beta) \mu_{\text{dis}}] + \left[\frac{1}{\beta / \mu_{\text{con}} + (1 - \beta) / \mu_{\text{dis}}} \right]}{2}, \quad (11)$$

where K_{cmb} and μ_{cmb} represent the weighted bulk and shear moduli of saturated rock, respectively.

Finally, according to the elastic moduli of saturated rock, the elastic parameters of rock (P-wave velocity $V_{\text{P-cmb}}$, S-wave velocity $V_{\text{S-cmb}}$ and density ρ) are computed as

$$V_{\text{P-cmb}} = \sqrt{\frac{K_{\text{cmb}} + \frac{4}{3} \mu_{\text{cmb}}}{\rho}}, \quad (12)$$

$$V_{\text{S-cmb}} = \sqrt{\frac{\mu_{\text{cmb}}}{\rho}}, \quad (13)$$

$$\rho = \phi (S_{\text{w}} \rho_{\text{w}} + (1 - S_{\text{w}}) \rho_{\text{h}}) + (1 - \phi) \rho_{\text{m}}, \quad (14)$$

where ρ_{w} , ρ_{m} , ρ_{h} and ρ are the brine, rock matrix, hydrocarbon, and bulk densities, respectively.

Due to the complexity of real rock structure, it is difficult to determine the content of connected or isolated pores at different depth ranges. In this regard, we define the percentage of connected pores β (the pore-connectivity parameter) as a pending variable and try to estimate it based on the observed P- and S-wave velocities of well log data.

Linearized Forward Operator

According to the established DEM-Gassmann rock-physics modeling process, porosity, water saturation and pore connectivity parameters are treated as objective variables, and the forward operator of quantitative correlation between the objective variables and elastic parameters can be expressed as

$$\mathbf{m} = \mathbf{F}(\mathbf{r}) + \mathbf{e}, \quad (15)$$

where $\mathbf{m}=[V_p, V_s, \rho]^T$ denotes the elastic parameters, $\mathbf{r}=[\phi, S_w, \beta]^T$ denotes the objective variables, \mathbf{F} denotes the forward operator by combining equations (1)-(14), and \mathbf{e} is the modeling error. The linearized forward model is obtained by performing a first-order Taylor approximation to equation (15),

$$\mathbf{c} = \mathbf{F}(\mathbf{r}_0) - \mathbf{D}\mathbf{r}_0, \quad (16)$$

$$\mathbf{c} = \mathbf{F}(\mathbf{r}_0) - \mathbf{D}\mathbf{r}_0, \quad (17)$$

where \mathbf{r}_0 represents the approximated objective variable for the Taylor approximation, \mathbf{c} is a constant that can be subtracted from the seismic elastic data \mathbf{m} during the calculations, and \mathbf{D} refers to the linearized forward operator,

$$\mathbf{D} = \left. \frac{\partial \mathbf{F}(\mathbf{r})}{\partial \mathbf{r}} \right|_{\mathbf{r}=\mathbf{r}_0} = \begin{bmatrix} \frac{\partial V_p}{\partial \phi} & \frac{\partial V_p}{\partial S_w} & \frac{\partial V_p}{\partial \beta} \\ \frac{\partial V_s}{\partial \phi} & \frac{\partial V_s}{\partial S_w} & \frac{\partial V_s}{\partial \beta} \\ \frac{\partial \rho}{\partial \phi} & \frac{\partial \rho}{\partial S_w} & \frac{\partial \rho}{\partial \beta} \end{bmatrix}_{\mathbf{r}=\mathbf{r}_0}. \quad (18)$$

The linear forward operator \mathbf{D} is the Jacobian matrix, which represents the partial derivatives of the seismic petrophysical forward operator \mathbf{F} with respect to \mathbf{r} . It can be referred with Appendix for the detailed expressions of these partial derivatives.

Rock Physics Inversion

From a statistical perspective, the reservoir parameters typically exhibit a multi-modal distribution due to variations in lithofacies and their physical properties. Hence, we employ a Gaussian mixture model (Grana *et al.* 2017) to represent the prior distribution. This prior distribution is expressed as the arithmetic average of Gaussian distributions,

$$P(\mathbf{\theta}) = \sum_{k=1}^C \phi_k N_k(\mathbf{r}; \mu_r^k, \Sigma_r^k), \quad (19)$$

where N_k represents the k th Gaussian distribution, μ_r^k , Σ_r^k , and ϕ_k are the mean, covariance, and weight coefficients of N_k , respectively, and C is the total number of Gaussian distributions. In practice, the Gaussian mixture model (mean, covariance, and weight coefficients) of the objective variables can be computed by using the expectation-maximization algorithm (Hastie *et al.* 2009), based on the sample data of pore connectivity parameter estimated from well-side P-/S-wave velocities and measured porosity and water saturation.

For the linearized model as expressed in equation (16), if we assume the data error exhibits a normal distribution with zero-mean $N(\mathbf{e}; 0, \Sigma_e)$, and the likelihood probability $P(\mathbf{m}|\mathbf{r})$ is determined by the linearized model, then the conditional probability $P(\mathbf{r}|\mathbf{m})$ also satisfies a Gaussian mixture distribution with the analytical expression (Grana *et al.* 2017) for the conditional mean,

$$\hat{\mathbf{r}}_{r|\mathbf{m}}^k = \mathbf{D}_r^k + \mu_r^k \mathbf{T} \left(\Sigma_r^k \mathbf{T} + \Sigma_e \right)^{-1} \left(-\mu_r^k \right), \quad (20)$$

$$\hat{\mathbf{D}}_{r|\mathbf{m}}^k = \mathbf{D}_r^k - \mu_r^k \mathbf{T} \left(\Sigma_r^k \mathbf{T} + \Sigma_e \right)^{-1} \mu_r^k \mathbf{T}. \quad (21)$$

The final inversion result of the objective variables is the weighted mean of the posterior mean

$$\hat{\mathbf{r}}_{\text{est}} = \sum_k \pi^k \hat{\mathbf{r}}_{r|\mathbf{m}}^k, \quad (22)$$

where

$$\pi^k(\mathbf{m}) = \frac{\phi_k N(\hat{\mathbf{r}}_{r|\mathbf{m}}^k; \hat{\mathbf{D}}_{r|\mathbf{m}}^k, \Sigma_r^k \mathbf{T} + \Sigma_e)}{\sum_h \phi_h N(\hat{\mathbf{r}}_{r|\mathbf{m}}^h; \hat{\mathbf{D}}_{r|\mathbf{m}}^h, \Sigma_r^h \mathbf{T} + \Sigma_e)}. \quad (23)$$

In practice, to improve computational efficiency, we employ the Bayesian linear inversion method based on the Aki-Richards approximation (Buland *et al.* 2003) for obtaining the elastic parameters of \mathbf{m} . Furthermore, considering that the linearized model heavily relies on the approximate points and initial models, we adopt an iterative Bayesian inversion method (Lang and Grana 2018) for subsequent inversions to improve the modeling accuracy. The posterior mean of Bayesian linear inversion is utilized as the initial model in each iteration of inversion process. The inversion process terminates until either the difference between the predicted and observed data falls below a pre-defined threshold or the maximum iterations are reached.

In summary, the proposed method involves the pore-connectivity parameter inversion and rock-physics modeling. The specific process of the proposed method is depicted in Figure 1. According to equation (19), the expectation-maximization algorithm is utilized for estimating the Gaussian mixture model.

The iterative Bayesian inversion, as per equations (20)-(23), is employed to obtain the objective variables. In practice, the number of Gaussian components is set to 2 assuming two lithofacies. The threshold for ending the iteration is set as 1% of the initial residual value and the maximum iteration is 10.

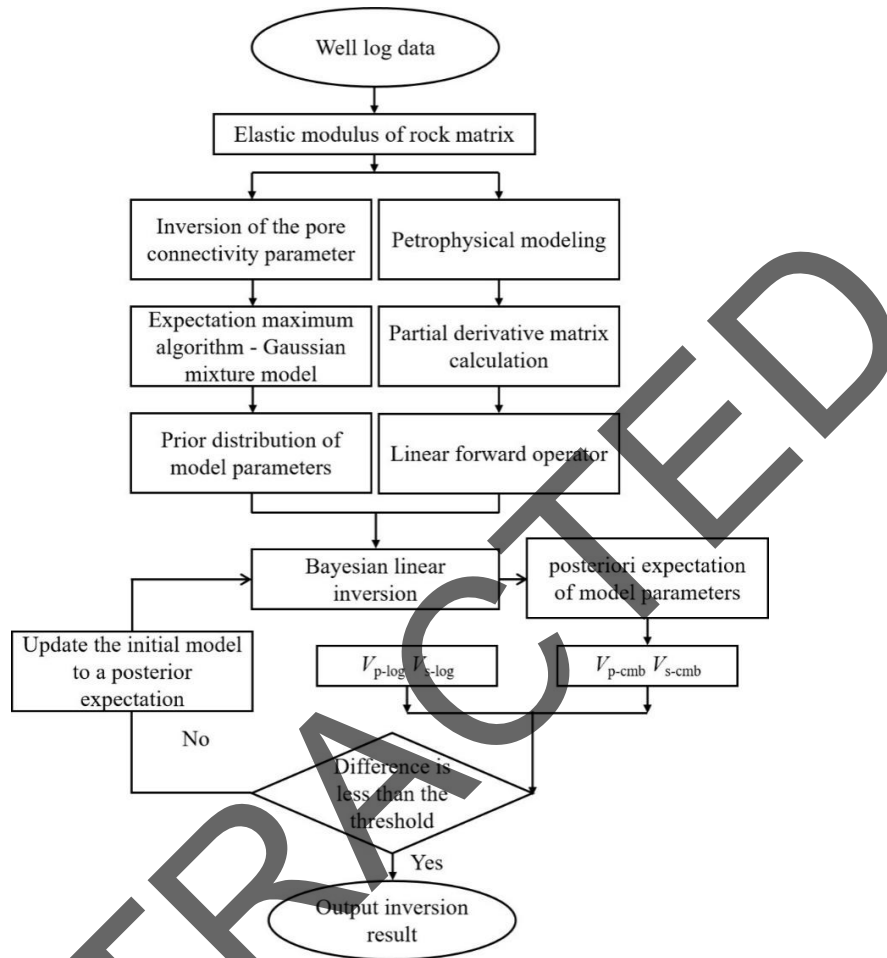


Figure 1. Flowchart of the seismic rock-physics inversion method for petrophysical and pore parameters

图中修改, Elastic moduli!

Posterior 还是 Posteriori!?

Well Log Data Test

The well logging data from a carbonate reservoir of northwest China have been selected for testing and verification. Figure 2 shows the log data of well A, including P- and S-wave velocities, density, porosity, and water saturation. The reservoir in this area primarily consists of karst carbonates, which exhibit complex crack and cavity distribution with strong heterogeneities. The identified target layer (2.045~2.072 s) is predominantly composed of pure dolomite with a minor presence of limestone □□□□. Table 1 presents the rock and fluid properties of carbonates. To describe the complex pore structure in carbonates, the proposed method reformulates the Xu-White model by combining the DEM

model and the Gassmann equation so as to incorporate the joint influences of isolated and connected pores. In the rock-physics modeling, the pore connectivity parameter represents the proportion of interconnected pores and serves as a weighting coefficient for adjusting the general elastic properties of different pore types in fluid-saturated rocks. In addition, such a pore parameter helps revealing the pore connectivity/permeability of carbonates to some extent, thereby improves the rock-physics modeling accuracy.

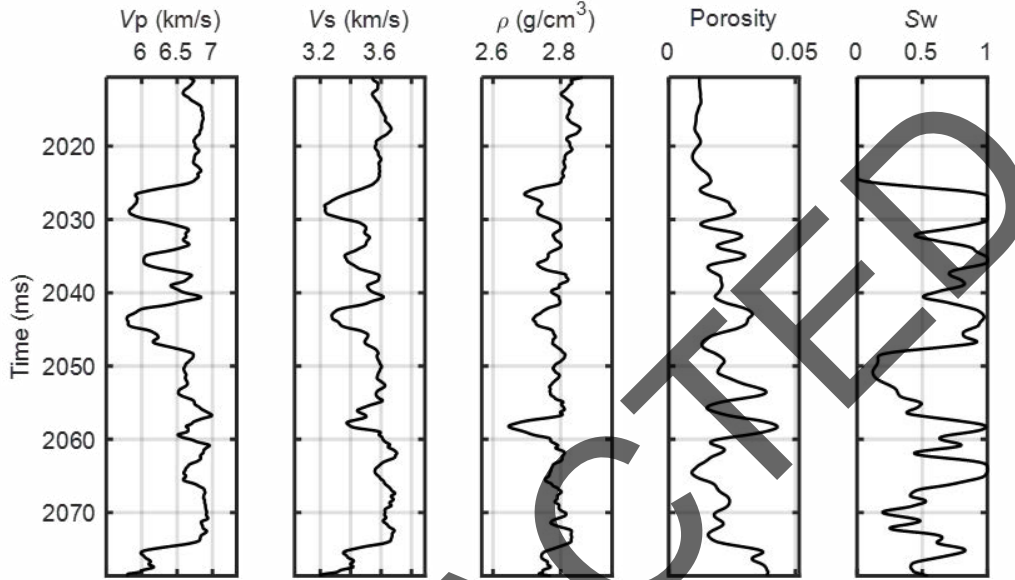


Figure 2. Well log data of (a) P-wave velocity, (b) S-wave velocity, (c) density, (d) porosity, and (e) water saturation.

Table 1 Rock and fluid properties for the carbonates.

	Dolomite	Limestone	Brine
Bulk modulus (GPa)	94	76.8	2.3
Shear modulus (GPa)	39	32	/
Density (g/cm ³)	2.87	2.71	1.05

Before the inversion, to illustrate the complexity of the pore structure of reservoirs, the Xu-White model is adopted as the connected-pore model, while the DEM model as the isolated-pore model to predict the elastic parameters around the well, respectively. The rock-physics modeling result with the conventional Xu-White model (with a constant pore aspect ratio of 0.15) is given in figure 3. By analyzing the prediction (see figure 3), it is apparent that the elastic parameters predicted by the conventional method exhibit the deviations from the log curve. The prediction gives the correlation coefficients of 0.8576 (V_p), 0.8264 (V_s), and 0.6367 (ρ) with respect to log data, and thereby only provide a general indication of the trend observed at the target layer.

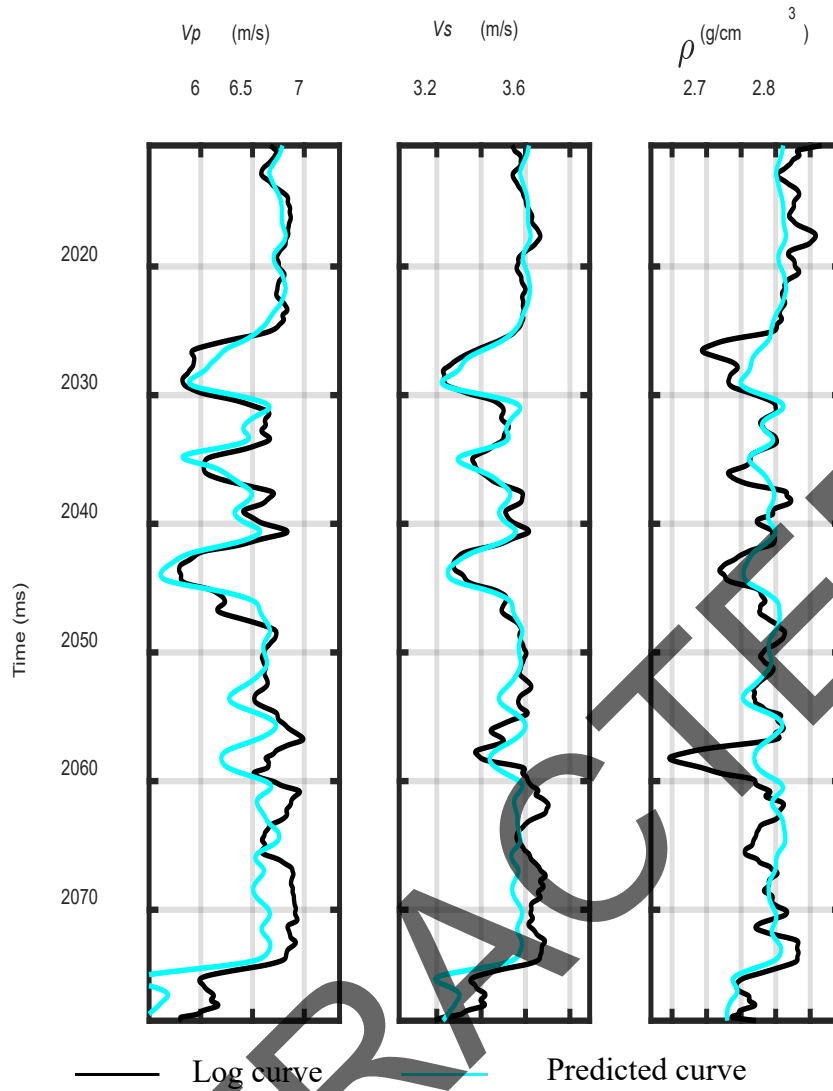


Figure 3. Predicted results of (a) P-wave velocity, (b) S-wave velocity, and (c) density by the conventional Xu-White model (connected-pore model) with a constant pore aspect ratio in comparison with the log curves.

For the comparison, the rock-physics modeling with the DEM model is shown in figure 4. By analyzing the results in figures 3 and 4, it is revealed that the prediction using only the connected-pore model (figure 3) generally underestimates the true value compared with the log data, whilst the isolated-pore model (figure 4) overestimates. For the connected-pore model, the stiffening effect caused by the isolated pores are neglected, and a softer rock frame is assumed. On the other hand, for the isolated-pore model, the equilibrium effect of pore fluid pressure gradient induced by elastic waves is neglected, so that no relaxation occurs. For each of the two models, there exists errors in the predictions due to the assumption of a single-porosity condition. The difference between the predicted and measured curves at some depths is obvious, which may cause the errors for the relevant rock-physics inversion.

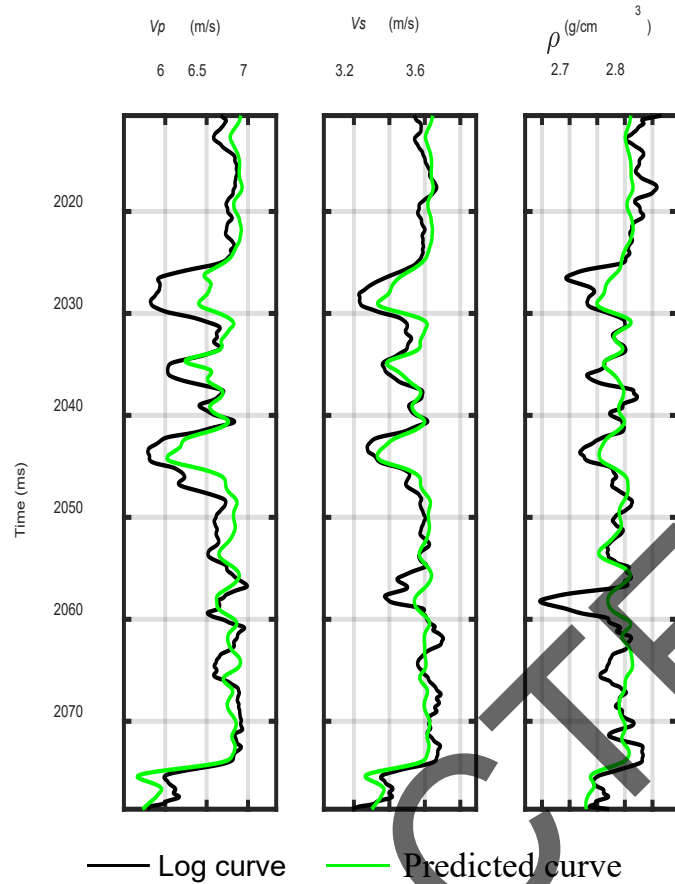


Figure 4. Predicted results of (a) P-wave velocity, (b) S-wave velocity, and (c) density by the DEM model (isolated-pore model) with a constant pore aspect ratio in comparison with the log curves.

The illustration in figures 3 and 4 indicates the conventional rock-physics modeling fails to provide a reasonable prediction of elastic properties for the carbonates with pore complexity. We hereby predict the pore-connectivity parameter based on equations (15)-(17), taking into account the overall elastic responses of the intricate pore structure. The pore-connectivity parameter estimated from the observed P- and S-wave velocities at well A is illustrated in figure 5d, based on which the velocities and density are predicted by the proposed method, along with a comparison with the log data (see figure 5a-c). Figure 6 overlaps the results predicted by the proposed method and that by the Xu-White model (figure 3), which shows that the proposed method achieves an apparent agreement with the log data (marked with the arrows in figure 6).

We also compare the proposed method with the method proposed by Guo *et al.* (2023). The latter (referred as the varying aspect-ratio method) addresses the pore complexity of carbonates by estimating the spatially-varying pore aspect ratio, which estimates the pore aspect ratio with observed P- and S-wave velocities based on the DEM model and the Gassmann equation under the Bayesian framework. Figure 7d shows the estimated pore aspect ratio of the study area, where the pore geometry reveals the spatial variation of reservoir pore types to a certain extent. Although, the prediction by the varying aspect-

ratio method generally matches well with the log data, the comparison between the two methods shows a slight improvement achieved by the proposed method (see figure 8). In summary, Table 2 shows the correlation coefficients between the log data and those predictions of figures 3, 5, and 7. The proposed method, which takes into account the interaction between connected and isolated pores, exhibits the best agreement (the highest correlation coefficient) with the well log data compared to both the varying aspect-ratio method (Guo *et al.* 2023) and the conventional Xu-White model.

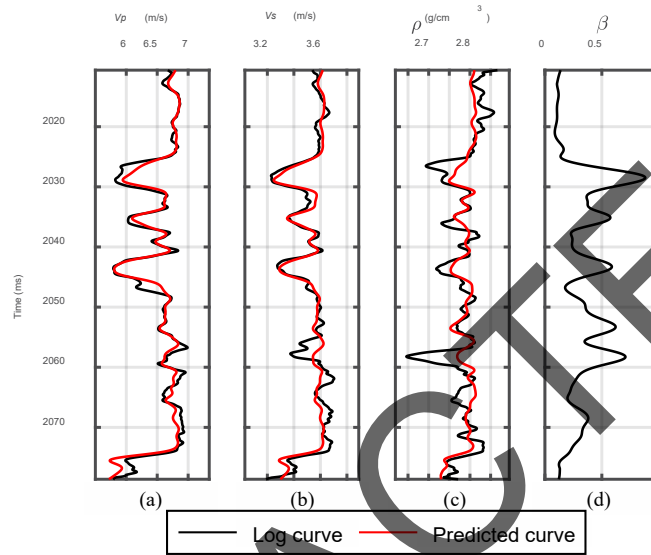


Figure 5. Predicted results of (a) P-wave velocity, (b) S-wave velocity, (c) density, and (d) pore connectivity parameter by the proposed method, in comparison with the log curves.

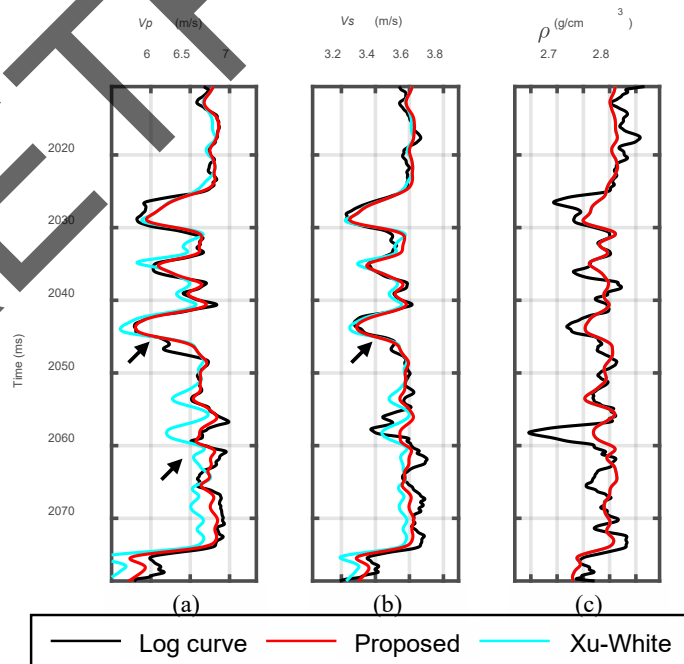


Figure 6. Comparison between the predicted results of (a) P-wave velocity, (b) S-wave velocity, and (c) density by the proposed method (red curves) and the Xu-White model (blue curves).

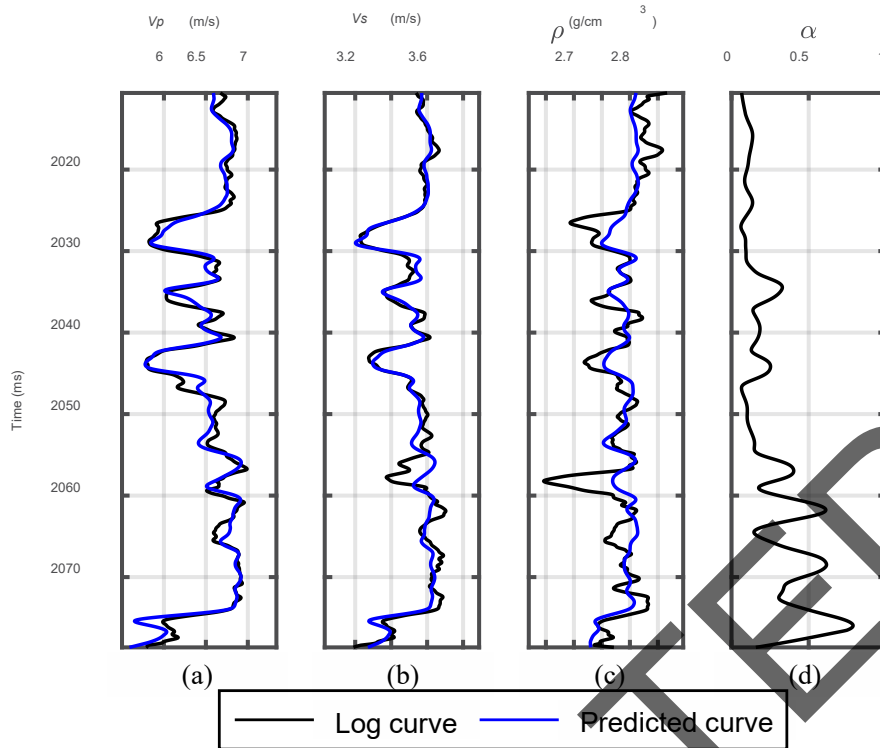


Figure 7. Predicted results of (a) P-wave velocity, (b) S-wave velocity, (c) density, and (d) pore aspect ratio by the method by Guo *et al.* (2023), in comparison with the log curves.

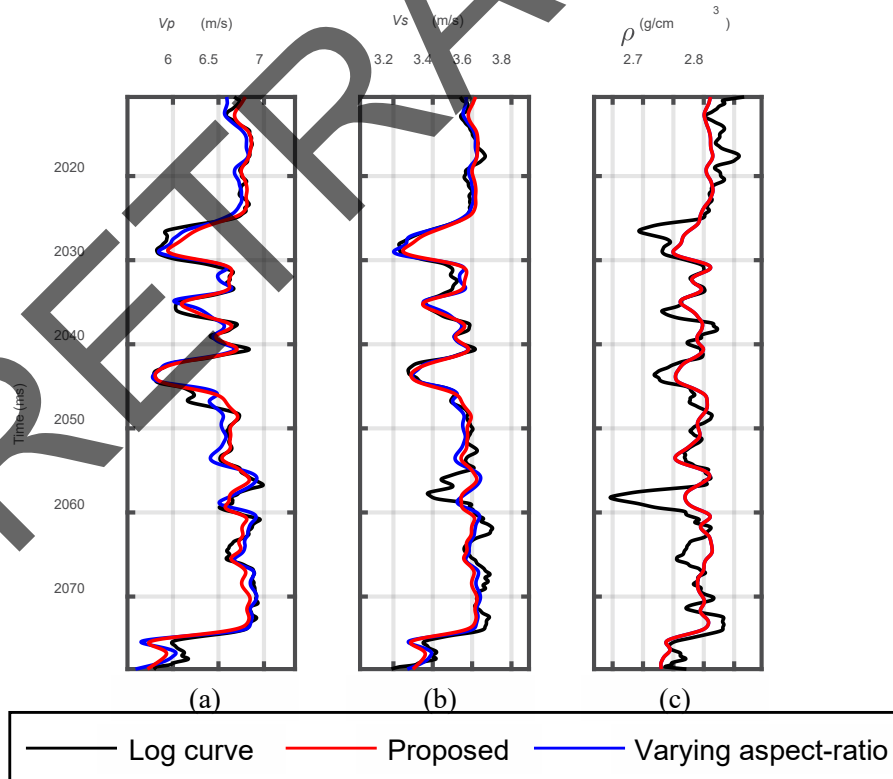


Figure 8. Comparison between the predicted results of (a) P-wave velocity, (b) S-wave velocity, and (c) density by the proposed method (red curves) and the method by Guo *et al.* (2023) (blue curves).

Table 2 Correlation coefficients between the log data and the predicted results of figures 3, 5, and 7.

	V_p	V_s
Xu-White model	0.8576	0.8264
Varying aspect-ratio method	0.9472	0.8905
Proposed model	0.9605	0.8908

Seismic Section Application

We apply the proposed method to the field seismic profile data obtained from a carbonate reservoir of southwest China. The field seismic data is from the same working area as the well log data in the previous tests. The reservoir pore space is complex and diverse, which has a great influence on the elastic properties of rocks. The proposed method which incorporates the variation of pore structures can be employed for predicting porosity and water saturation as well as the pore-connectivity parameter. Furthermore, it enables the evaluation of favorable reservoir areas within the work area. The survey line crossing the two wells is extracted for the application, which is shown in figure 9. The target layer has a depth range of approximately 4610-4704 m, with the corresponding time depth range of 2072-2045ms at well B.

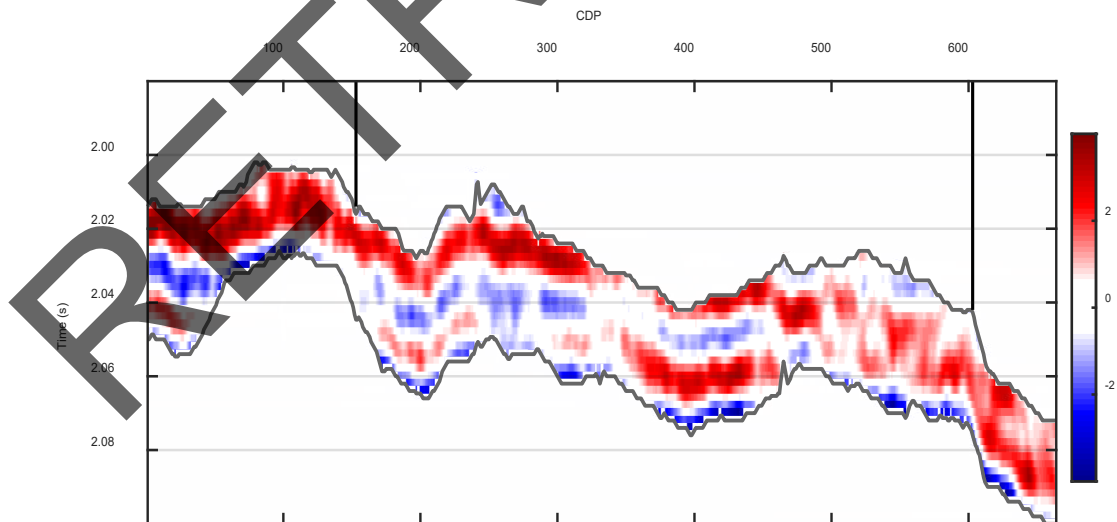


Figure 9. Stacked seismic section of the 2D survey line with the two wells located at the 165 and 601 CDPs.

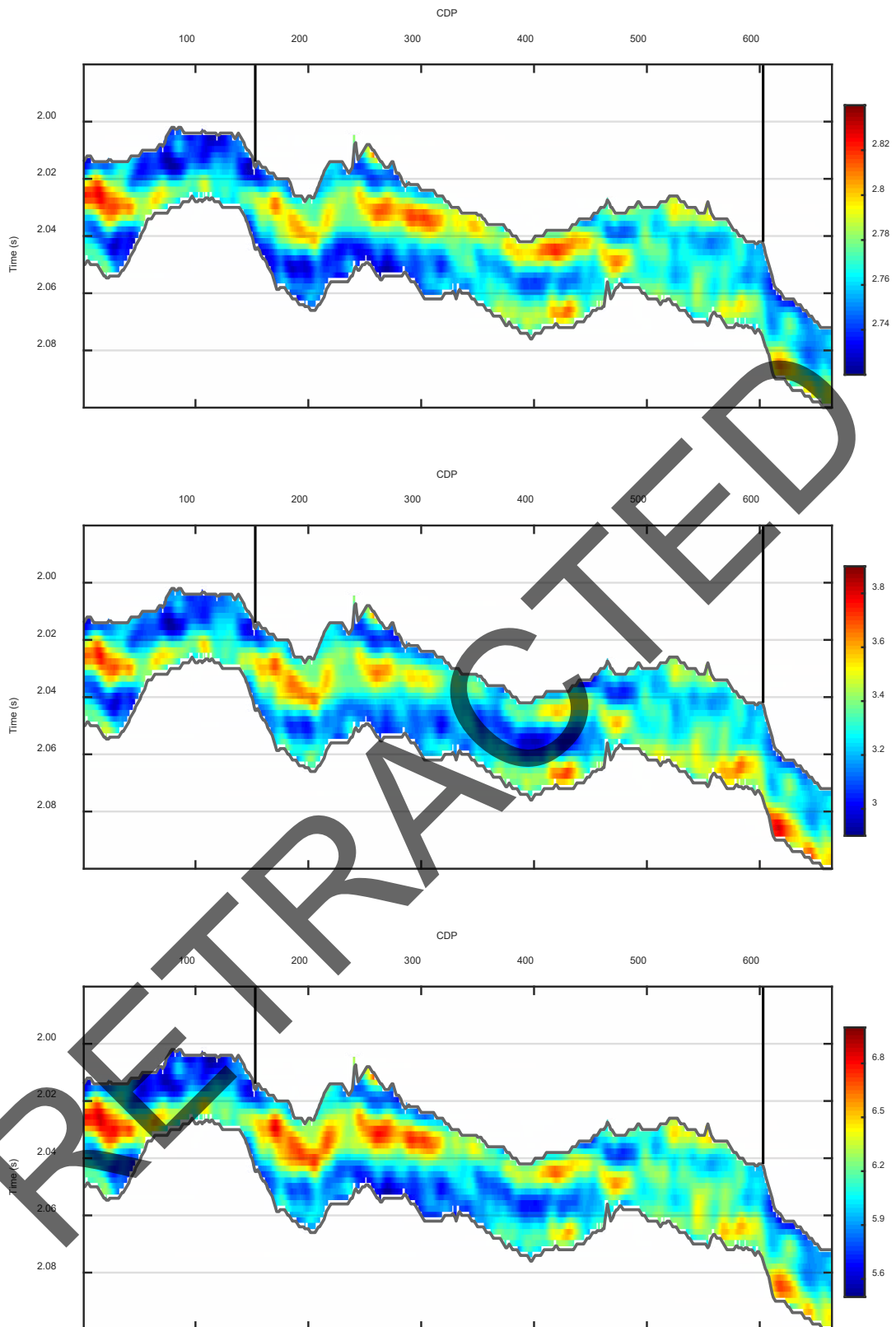


Figure 10. Sections of P- (a) and S- (b) wave velocities and density (c) from prestack seismic inversion for the survey line.

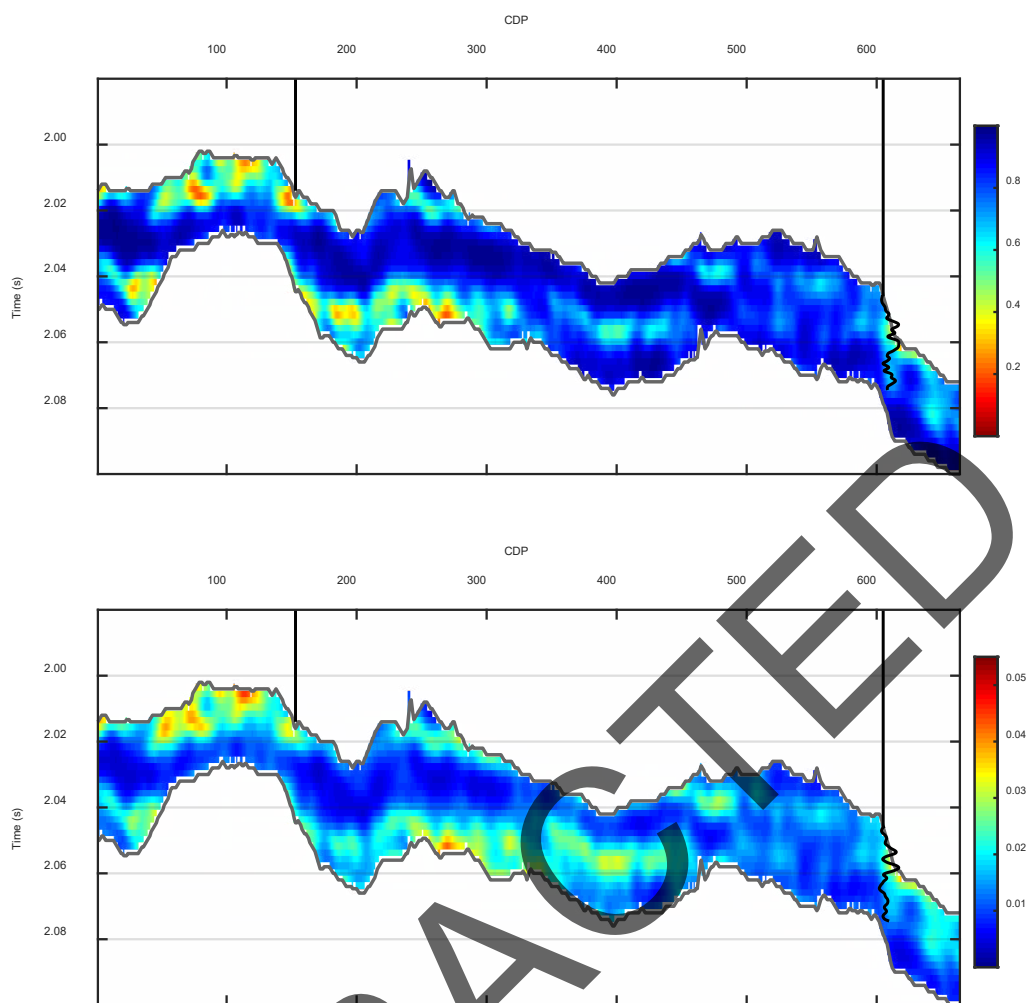


Figure 11. Inversion results of (a) porosity and (b) water saturation by the proposed method for the survey line.

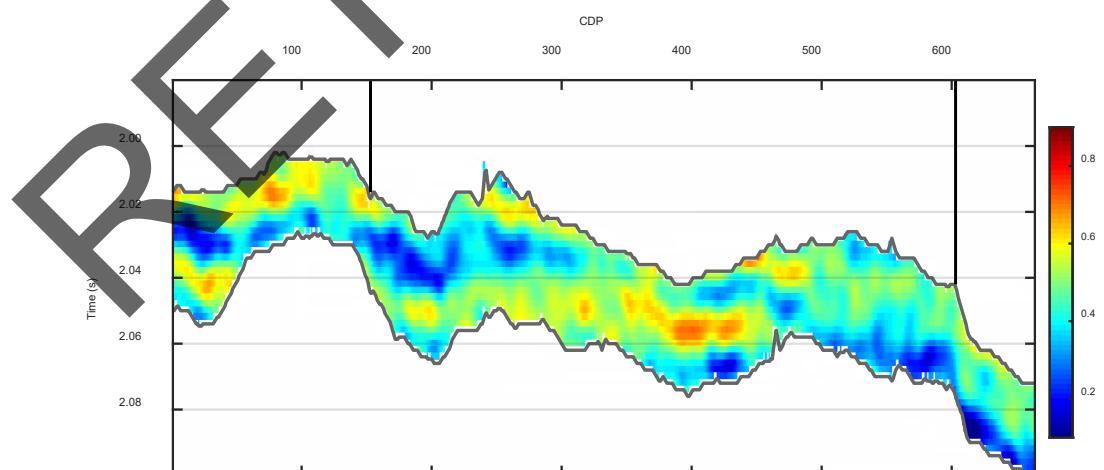


Figure 12. Inversion result of pore-connectivity parameter by the proposed method for the survey line.

The elastic data of P-/S-wave velocities and density sections (figure 10) are obtained through the prestack seismic inversion (Buland *et al.* 2003) of the survey line. Based on the elastic data, the porosity, water saturation, and pore connectivity parameters are simultaneously inverted by using the proposed method. The prediction results of porosity and water saturation are shown in figure 11. Wells A and B were utilized for the validation of the inverted sections. Based on the production reports, the gas test results indicate that well B is a highly productive gas well, producing 1.047 million m³/d of gas, while well A has a water production rate of 591 m³/d. In the prediction results of figure 11, the zone of high porosity and low water saturation area (~165 CDP) is generally consistent with the proven gas bearing reservoir of well A; the high water saturation area (~600 CDP, figure 11b) also accords with the location of well B (water producing). Besides, figure 12 shows the section of inverted pore-connectivity parameter. Although the inverted result can not be verified since there is no observed pore connectivity data, it indicates the relatively high connectivity around the production well. The inverted petrophysical and pore parameters can be helpful in identifying the potential gas reservoirs.

CONCLUSION

The present study proposes a rock-physics modeling and inversion method for carbonate reservoirs which considers the impacts of different pore types (connected and isolated pores) on the elastic properties. The elastic properties of fluid-saturated rocks are often underestimated or overestimated due to the presence of connected or isolated pores. In this regard, the DEM model can be employed to account for the influence of isolated pores on fluid-containing rocks while the Xu-White model for the connected pores. Based on the rock-physics modeling, the seismic petrophysical inversion is proposed to jointly estimate petrophysical and pore-connectivity parameters.

Compared with the conventional Xu-White model that assumes fully-connected pores, the predicted P- and S-wave velocities by the proposed method show an improved agreement with the well log data. The proposed method is also compared with the modeling method with spatially-varying pore aspect ratio, which shows the good performance on capturing pore complexity in carbonates. The application of seismic survey line validates the validity of the method, and the inversion results for porosity and water saturation effectively indicate the spatial distribution of favorable reservoirs. The estimated pore-connectivity parameter can assist with identifying gas-bearing regions being characterized by the relatively higher permeability.

However, the linearized model is unable to fully capture the highly nonlinear relationships between the petrophysical properties and elastic parameters, so the modeling accuracy is limited under the certain conditions. The pore-connectivity parameter serves as an auxiliary variable that accounts for the effects of different pore types, which fails to accurately depict the intricate details of pore structure within carbonate rocks.

ACKNOWLEDGEMENTS

This work is supported by the National Natural Science Foundation of China (grant nos. 41974123, 42174161, 42104128), and the Jiangsu Innovation and Entrepreneurship Plan.

Conflict of interest statement. The authors declare that there is no conflict of interest for this work.

REFERENCES

- Assefa, S., McCann, C., and Sothcott, J., 2003. Velocities of compressional and shear waves in limestones. *Geophysical Prospecting*, 51(1), 1–13. <https://doi.org/10.1046/j.1365-2478.2003.00349.x>
- Azevedo, L., Nunes, R., Soares, A., et al., 2018. Geostatistical seismic amplitude-versus-angle inversion. *Geophysical Prospecting*, 66, 116–131. <https://doi.org/10.1111/1365-2478.12589>
- Ba, J., Xu, W., Fu, L.Y., José, M.C., and Zhang, L., 2017. Rock anelasticity due to patchy-saturation and fabric heterogeneity: A double double-porosity model of wave propagation. *Journal of Geophysical Research: Solid Earth*, 122, 1949–1971. <https://doi.org/10.1002/2016JB013882>
- Bemer, E., Hamon, Y., Adelinet, M., 2019. Consistent experimental investigation of the applicability of Biot-Gassmann's equation in carbonates. *Geophysics*, 84(4), WA97–WA113. <https://doi.org/10.1190/geo2018-0631.1>
- Berryman, J.G., 1980. Long-wavelength propagation in composite elastic media II. Ellipsoidal inclusions. *Journal of the Acoustical Society of America*, 68(6), 1820–1831. <https://doi.org/10.1121/1.385172>
- Buland, A., Omre, H., 2003. Bayesian linearized AVO inversion. *Geophysics*, 68(1), 185–198. <https://doi.org/10.1190/1.1543206>
- Cao, Z.N., Li, X.Y., Liu, J., Qin, X.L., Sun, S.H., Li, Z.J., Cao, Z.Y., 2018. Carbonate fractured gas reservoir prediction based on P-wave azimuthal anisotropy and dispersion. *Journal of Geophysics and Engineering*, 15(5), 2139–2149. <https://doi.org/10.1088/1742-2140/aabe58>
- Carcione, J.M., Helle, H.B., Avseth, P., 2011. Source-rock seismic velocity models: Gassmann versus Backus. *Geophysics*, 76(5), N37–N45. <https://doi.org/10.1190/GEO2010-0258.1>
- Chen, H.Z., Pan, X.P., Ji, Y.X., and Zhang, G.Z., 2017. Bayesian Markov Chain Monte Carlo inversion for weak anisotropy parameters and fracture weaknesses using azimuthal elastic impedance. *Geophysical Journal International*, 210, 801–818. <https://doi.org/10.1093/gji/ggx196>
- Cleary, M.P., Chen, I.W., and Lee, S.M., 1980. Self-consistent techniques for heterogeneous media. *Journal of Engineering Mechanics*, 106(5), 861–887. <https://doi.org/10.1243/03093247V154235>
- Dias, C.H., Eler, F.M., Cordeiro, C., Ramirez, M.G., Soares, J.A., Nunes, D., Lima, M.C.O., Couto, P., 2023. Effects of pore size and pore connectivity on trapped gas saturation. *Journal of Hydrology and Hydromechanics*, 71

- (1), 11–21. <https://doi.org/10.2478/johh-2022-0042>
- Falahat, R., and Farrokhnia, F., 2020. Rock physics modelling of the carbonate reservoirs: A log-based algorithm to determine the pore aspect ratio. *Journal of Applied Geophysics*, 173, 103930. <https://doi.org/10.1016/j.jappgeo.2019.103930>
- Fjeldstad, T., and Omre, H., 2020. Bayesian inversion of convolved hidden Markov models with applications in reservoir prediction. *IEEE Transactions on Geoscience and Remote Sensing*, 58, 1957–1968. <https://doi.org/10.1109/TGRS.2019.2951205>
- Garia, S., Pal, A.K., Ravi, K., and Nair, A.M., 2021. Laboratory assessment on factors controlling the acoustic properties of carbonates: A case study from Bombay offshore. *Journal of Petroleum Science and Engineering*, 203, 108607. <https://doi.org/10.1016/j.petrol.2021.108607>
- Gassmann, F., 1951. Elastic waves through a packing of spheres. *Geophysics*, 16(4), 673–685. <https://doi.org/10.1190/1.1437718>
- Gharechelou, S., Amini, A., Kadkhodaie-Ilkhchi, A., Moradi, B., 2015, An integrated approach for determination of pore-type distribution in carbonate-siliciclastic Asmari Reservoir, Cheshmeh- Khosh Oilfield, SW Iran. *Journal of Geophysics and Engineering*, 12(5), 793–809. <https://doi.org/10.1088/1742-2132/12/5/793>
- Grana, D., 2016. Bayesian linearized rock-physics inversion. *Geophysics*, 81, D625–D641. <https://doi.org/10.1190/geo2016-0161.1>
- Grana, D., Fjeldstad, T., Omre, H., 2017. Bayesian Gaussian mixture linear inversion for geophysical inverse problems. *Mathematical Geosciences*, 49, 493–515. <https://doi.org/10.1007/s11004-016-9671-9>
- Gunning, J., and Glinsky, M., 2007. Detection of reservoir quality using Bayesian seismic inversion: *Geophysics*, 72, R37–R49. <https://doi.org/10.1190/1.2713043>
- Guo, Q., Ba, J., and Luo C., 2022. Nonlinear petrophysical amplitude variation with offset inversion inversion with spatially-variable pore aspect ratio. *Geophysics*, 87(4), M111–M125. <https://doi.org/10.1190/geo2021-0583.1>
- Guo, Q., Ba, J., Luo, C., 2023. Seismic rock-physics linearized inversion for reservoir-property and pore-type parameters with application to carbonate reservoirs. *Geoenergy Science and Engineering*, 224, 211640. <https://doi.org/10.1016/j.geoen.2023.211640>
- Hastie, T., Tibshirani, R., Friedman, J., 2009. The Elements of Statistical Learning. *Springer Series in Statistics*. <https://doi.org/10.1007/978-0-387-84858-7>
- Hill, R., 1952. The elastic behaviour of a crystalline aggregate. *Proceedings of the Physical Society. Section A*, 65(5), 349–354. <https://doi.org/10.1088/0370-1298/65/5/307>
- Ishola, O., Alexander, A., Vilcáez, J., 2022. Statistical and neural network analysis of the relationship between the stochastic nature of pore connectivity and flow properties of heterogeneous rocks. *Journal of Natural Gas Science and Engineering*, 105. <https://doi.org/10.1016/j.jngse.2022.104719>

- Ji, L.X., and Zong, Z.Y., 2023, Lithology discrimination based on direct inversion of Poisson impedance for deep tight-sandstone reservoirs. *Journal of Geophysics and Engineering*, 20(1), 38–48. <https://doi.org/10.1093/jge/gxac092>
- Keys, R. G., and Xu, S., 2002. An approximation for the xu-white velocity model. *Geophysics*, 67(5), 1406–1414. <https://doi.org/10.1190/1.1815784>
- Kuster, G.T., and Toksöz, M.N., 1974. Velocity and attenuation of seismic waves in two-phase media: Part I. Theoretical formulations. *Geophysics*, 39(5), 587. <https://doi.org/10.1190/1.1440450>
- Lang, X., and Grana, D., 2018. Bayesian linearized petrophysical AVO inversion. *Geophysics*, 83, M1–M13. <https://doi.org/10.1190/geo2017-0364.1>
- Luo, C., Ba, J., and Guo, Q., 2023. Probabilistic seismic petrophysical inversion with statistical double-porosity Biot-Rayleigh model. *Geophysics*, 88(3), M157–M171. <https://doi.org/10.1190/geo2022-0288.1>
- Markov, M., Kazatchenko, E., Mousatov, A., and Pervago, E., 2013. Novel approach for simulating the elastic properties of porous rocks including the critical porosity phenomena. *Geophysics*, 78(4), L37–L44. <https://doi.org/10.1190/geo2012-0260.1>
- Mirkamali, M.S., Javaherian, A., Hassani, H., et al., 2020. Quantitative pore-type characterization from well logs based on the seismic petrophysics in a carbonate reservoir. *Geophysical Prospecting*, 68, 2195–2216. <https://doi.org/10.1111/1365-2478.12989>
- Norris, A.N., 1985. A differential scheme for the effective moduli of composites. *Mechanics of Materials*, 4(1), 1–16. [https://doi.org/10.1016/0167-6636\(85\)90002-X](https://doi.org/10.1016/0167-6636(85)90002-X)
- Pan, X.P., Zhang, G.Z., and Yin, X.Y., 2019. Linearized amplitude variation with offset and azimuth and anisotropic poroelasticity. *Geophysical Prospecting*, 67(7), 1882–1897. <https://doi.org/10.1111/1365-2478.12778>
- Panizza, G., Ravazzoli, C., 2019, An efficient rock-physics workflow for modeling and inversion in anisotropic organic-shales. *Journal of Petroleum Science and Engineering*, 180, 1101–1111. <https://doi.org/10.1016/j.petrol.2019.06.005>
- Qin, Z.Y., Wen, X.T., Zhou, D.Y., et al., 2022. Inversion method of elastic and fracture parameters of shale reservoir with a set of inclined fractures. *IEEE Transactions on Geoscience and Remote Sensing*, 60, 4507213. <https://doi.org/10.1109/TGRS.2021.3138750>
- Wang, P., Li, J.Y., Chen, X.H., Wang, B.F., 2020, Joint probabilistic fluid discrimination of tight sandstone reservoirs based on Bayes discriminant and deterministic rock physics modeling. *Journal of Petroleum Science and Engineering*, 191, 103930. <https://doi.org/10.1016/j.petrol.2020.107218>
- Weger, R.J., Eberli, G.P., Baechle, G.T., Massaferro, J.L., and Sun, Y.F., 2009. Quantification of pore structure and its effect on sonic velocity and permeability in carbonates. *AAPG Bulletin*, 93(10), 1297–1317. <https://doi.org/10.1306/05270909001>

- Xu, S., and Payne, M.A., 2009. Modeling elastic properties in carbonate rocks. *The Leading Edge*, 28(1), 66–74. <https://doi.org/10.1190/1.3064148>
- Xu, S., White, R.E., 1995. A new velocity model for clay-sand mixtures. *Geophysical Prospecting*. 43, 91-118. <https://doi.org/10.1111/j.1365-2478.1995.tb00126.x>
- Yin, X.Y., Sun, R.Y., Wang, B.L., and Zhang, G.Z., 2014. Simultaneous inversion of petrophysical parameters based on geostatistical a priori information. *Applied Geophysics*, 11(3), 311–320. <https://doi.org/10.1007/s11770-014-0445-1>
- Zhang, S.X., Zou, C.C., Peng C., Yan, L.W., Wu, X.W., 2022, Pore structure and its effect on acoustic velocity and permeability of reef-shoal carbonates in the Tarim Basin, Northwest China. *Journal of Geophysics and Engineering*, 19(6), 1340–1354. <https://doi.org/10.1093/jge/gxac087>
- Zhang, Y.X., Yang, S.L., Zhang, Z. et al., 2022. Multiscale pore structure characterization of an ultra-deep carbonate gas reservoir. *Journal of Petroleum Science and Engineering*, 208(D), 109751. <https://doi.org/10.1016/j.petrol.2021.109751>
- Zimmerman, R.W., 1985. The effect of microcracks on the elastic moduli of brittle materials. *Journal of Materials Science Letters*, 4(12), 1457–1460. <https://doi.org/10.1007/BF00721363>

Appendix. Partial Derivative of Linearized Forward Model

$$\frac{\partial V_p}{\partial \phi} = \frac{1}{2V_p \rho^2} \left[\left(\frac{\partial K_{\text{cmb}}}{\partial \phi} + \frac{4}{3} \frac{\partial \mu_{\text{cmb}}}{\partial \phi} \right) \rho - \frac{\partial \rho}{\partial \phi} \left(K_{\text{cmb}} + \frac{4}{3} \mu_{\text{cmb}} \right) \right], \quad (1)$$

where

$$\begin{aligned} \frac{\partial K_{\text{cmb}}}{\partial \phi} = & \frac{1}{2} \beta \frac{\partial K_{\text{con}}}{\partial \phi} + \frac{1}{2} \frac{\partial K_{\text{dis}}}{\partial \phi} - \frac{1}{2} \beta \frac{\partial K_{\text{dis}}}{\partial \phi} + \frac{1}{2} [\beta K_{\text{dis}} + (1-\beta) K_{\text{con}}]^{-1} \\ & \times \left(\frac{\partial K_{\text{con}}}{\partial \phi} K_{\text{dis}} + \frac{\partial K_{\text{dis}}}{\partial \phi} K_{\text{con}} \right) - \frac{1}{2} K_{\text{con}} K_{\text{dis}} [\beta K_{\text{dis}} + (1-\beta) K_{\text{con}}]^{-2} \left[\beta \frac{\partial K_{\text{dis}}}{\partial \phi} + (1-\beta) \frac{\partial K_{\text{con}}}{\partial \phi} \right], \end{aligned} \quad (2)$$

and

$$\frac{\partial K_{\text{con}}}{\partial \phi} = \frac{\partial K_d}{\partial \phi} - 2 \left(1 - \frac{K_d}{K_m} \right) \frac{1}{K_m} \frac{\partial K_d}{\partial \phi} \left(\frac{\beta \phi}{K_f} + \frac{1-\beta \phi}{K_m} - \frac{K_d}{K_m^2} \right)^{-1}, \quad (3)$$

$$\begin{aligned} & - \left(1 - \frac{K_d}{K_m} \right)^2 \left(\frac{\beta \phi}{K_f} + \frac{1-\beta \phi}{K_m} - \frac{K_d}{K_m^2} \right)^{-2} \left(\frac{\beta}{K_f} - \frac{\beta}{K_m} - \frac{1}{K_m^2} \frac{\partial K_d}{\partial \phi} \right) \\ & \frac{\partial K_{\text{dis}}}{\partial \phi} = K_m P (\beta - 1) [1 - (1-\beta) \phi]^{P-1}. \end{aligned} \quad (4)$$

The partial derivative of P-wave velocity with respect to water saturation is

$$\frac{\partial V_p}{\partial S_w} = \frac{1}{2V_p \rho^2} \left[\frac{\partial K_{\text{cmb}}}{\partial S_w} \rho - \frac{\partial \rho}{\partial S_w} \left(K_{\text{cmb}} + \frac{4}{3} \mu_{\text{cmb}} \right) \right], \quad (5)$$

where

$$\begin{aligned} \frac{\partial K_{\text{cmb}}}{\partial S_w} = & \frac{1}{2} \beta \frac{\partial K_{\text{con}}}{\partial S_w} + \frac{1}{2} \frac{\partial K_{\text{dis}}}{\partial S_w} - \frac{1}{2} \beta \frac{\partial K_{\text{dis}}}{\partial S_w} + \frac{1}{2} [\beta K_{\text{dis}} + (1-\beta) K_{\text{con}}]^{-1} \\ & \times \left(\frac{\partial K_{\text{con}}}{\partial S_w} K_{\text{dis}} + \frac{\partial K_{\text{dis}}}{\partial S_w} K_{\text{con}} \right) - \frac{1}{2} K_{\text{con}} K_{\text{dis}} [\beta K_{\text{dis}} + (1-\beta) K_{\text{con}}]^{-2} \left[\beta \frac{\partial K_{\text{dis}}}{\partial S_w} + (1-\beta) \frac{\partial K_{\text{con}}}{\partial S_w} \right], \end{aligned} \quad (6)$$

and

$$\frac{\partial K_{\text{con}}}{\partial S_w} = \left(1 - \frac{K_d}{K_w} \right)^2 \left(\frac{\beta \phi}{K_f} + \frac{1-\beta \phi}{K_m} - \frac{K_d}{K_m^2} \right)^{-2} \frac{\beta \phi}{K_f^2} \frac{\partial K_f}{\partial S_w}. \quad (7)$$

The partial derivative of P-wave velocity with respect to pore- connectivity parameter is

$$\frac{\partial V_p}{\partial \beta} = \frac{1}{2V_p \rho} \left(\frac{\partial K_{\text{cmb}}}{\partial \beta} + \frac{4}{3} \frac{\partial \mu_{\text{cmb}}}{\partial \beta} \right), \quad (8)$$

where

$$\begin{aligned} \frac{\partial K_{\text{cmb}}}{\partial \beta} = & \frac{1}{2} K_{\text{con}} + \frac{1}{2} \beta \frac{\partial K_{\text{con}}}{\partial \beta} + \frac{1}{2} \frac{\partial K_{\text{dis}}}{\partial \beta} - \frac{1}{2} K_{\text{dis}} - \frac{1}{2} \beta \frac{\partial K_{\text{dis}}}{\partial \beta} \\ & + \frac{1}{2} \left(\frac{\partial K_{\text{con}}}{\partial \beta} K_{\text{dis}} + \frac{\partial K_{\text{dis}}}{\partial \beta} K_{\text{con}} \right) [\beta K_{\text{dis}} + (1-\beta) K_{\text{con}}]^{-1}, \\ & - \frac{1}{2} K_{\text{con}} K_{\text{dis}} [\beta K_{\text{dis}} + (1-\beta) K_{\text{con}}]^{-2} \left[K_{\text{dis}} + \beta \frac{\partial K_{\text{dis}}}{\partial \beta} - K_{\text{con}} + (1-\beta) \frac{\partial K_{\text{con}}}{\partial \beta} \right] \end{aligned} \quad (9)$$

and

$$\frac{\partial K_{\text{con}}}{\partial \beta} = - \left(1 - \frac{K_d}{K_m} \right)^2 \left(\frac{\beta \phi}{K_f} + \frac{1-\beta \phi}{K_m} - \frac{K_d}{K_m^2} \right)^{-2} \left(\frac{\phi}{K_f} - \frac{\phi}{K_m} \right), \quad (10)$$

$$\frac{\partial K_{\text{dis}}}{\partial \beta} = K_m P \phi [1 - (1 - \beta)\phi]^{p-1}, \quad (11)$$

where

$$\frac{\partial K_d}{\partial \phi} = K_m P (-1)(1 - \phi)^{p-1}. \quad (12)$$

The partial derivative of S-wave velocity with respect to porosity is

$$\frac{\partial V_s}{\partial \phi} = \frac{1}{2V_s \rho^2} \left(\frac{\partial \mu_{\text{cmb}}}{\partial \phi} \rho - \frac{\partial \rho}{\partial \phi} \mu_{\text{cmb}} \right), \quad (13)$$

where

$$\begin{aligned} \frac{\partial \mu_{\text{cmb}}}{\partial \phi} &= \frac{1}{2} \beta \frac{\partial \mu_{\text{con}}}{\partial \phi} + \frac{1}{2} \frac{\partial \mu_{\text{dis}}}{\partial \phi} - \frac{1}{2} \beta \frac{\partial \mu_{\text{dis}}}{\partial \phi} + \frac{1}{2} [\beta \mu_{\text{dis}} + (1 - \beta) \mu_{\text{con}}]^{-1} \\ &\times \left(\frac{\partial \mu_{\text{con}}}{\partial \phi} \mu_{\text{dis}} + \frac{\partial \mu_{\text{dis}}}{\partial \phi} \mu_{\text{con}} \right) - \frac{1}{2} \mu_{\text{con}} \mu_{\text{dis}} [\beta \mu_{\text{dis}} + (1 - \beta) \mu_{\text{con}}]^{-2} \left[\beta \frac{\partial \mu_{\text{dis}}}{\partial \phi} + (1 - \beta) \frac{\partial \mu_{\text{con}}}{\partial \phi} \right], \end{aligned} \quad (14)$$

and

$$\frac{\partial \mu_{\text{con}}}{\partial \phi} = \frac{\partial \mu_d}{\partial \phi}, \quad (15)$$

$$\frac{\partial \mu_{\text{dis}}}{\partial \phi} = \mu_m Q (\beta - 1) [1 - (1 - \beta)\phi]^{q-1}. \quad (16)$$

The partial derivative of S-wave velocity with respect to water saturation is

$$\frac{\partial V_s}{\partial S_w} = \frac{1}{2V_s \rho^2} \left(\frac{\partial \mu_{\text{cmb}}}{\partial S_w} \rho - \frac{\partial \rho}{\partial S_w} \mu_{\text{cmb}} \right), \quad (17)$$

where

$$\begin{aligned} \frac{\partial \mu_{\text{cmb}}}{\partial S_w} &= \frac{1}{2} \beta \frac{\partial \mu_{\text{con}}}{\partial S_w} + \frac{1}{2} \frac{\partial \mu_{\text{dis}}}{\partial S_w} - \frac{1}{2} \beta \frac{\partial \mu_{\text{dis}}}{\partial S_w} + \frac{1}{2} [\beta \mu_{\text{dis}} + (1 - \beta) \mu_{\text{con}}]^{-1} \\ &\times \left(\frac{\partial \mu_{\text{con}}}{\partial S_w} \mu_{\text{dis}} + \frac{\partial \mu_{\text{dis}}}{\partial S_w} \mu_{\text{con}} \right) - \frac{1}{2} \mu_{\text{con}} \mu_{\text{dis}} [\beta \mu_{\text{dis}} + (1 - \beta) \mu_{\text{con}}]^{-2} \left[\beta \frac{\partial \mu_{\text{dis}}}{\partial S_w} + (1 - \beta) \frac{\partial \mu_{\text{con}}}{\partial S_w} \right]. \end{aligned} \quad (18)$$

The partial derivative of S-wave velocity with respect to pore-connectivity parameter is

$$\frac{\partial V_s}{\partial \beta} = \frac{1}{2V_s \rho} \frac{\partial \mu_{\text{cmb}}}{\partial \beta}, \quad (19)$$

where

$$\begin{aligned} \frac{\partial \mu_{\text{cmb}}}{\partial \beta} &= \frac{1}{2} \mu_{\text{con}} + \frac{1}{2} \frac{\partial \mu_{\text{dis}}}{\partial \beta} - \frac{1}{2} \mu_{\text{con}} - \frac{1}{2} \beta \frac{\partial \mu_{\text{dis}}}{\partial \beta} + \frac{1}{2} \frac{\partial \mu_{\text{dis}}}{\partial \beta} \mu_{\text{con}} [\beta \mu_{\text{dis}} + (1 - \beta) \mu_{\text{con}}]^{-1} \\ &- \frac{1}{2} \mu_{\text{con}} \mu_{\text{dis}} \left[\mu_{\text{dis}} + \beta \frac{\partial \mu_{\text{dis}}}{\partial \beta} - \mu_{\text{con}} \right]^{-2}, \end{aligned} \quad (20)$$

and

$$\frac{\partial \mu_{\text{dis}}}{\partial \beta} = \mu_m Q \phi [1 - (1 - \beta)\phi]^{q-1}. \quad (21)$$